Engineering Structures 156 (2018) 161–174

Contents lists available at ScienceDirect

Engineering Structures

journal homepage: www.elsevier.com/locate/engstruct

Effect of yield penetration on column plastic hinge length

K.G. Megalooikonomou[a,*], S.P. Tastani[b], S.J. Pantazopoulou[c]

[a] University of Cyprus (UCY), 75 Kallipoleos Street, P.O. Box 20537, 1687 Nicosia, Cyprus
[b] Democritus University of Thrace (DUTh), Kimmeria Campus, Building B, Xanthi 67100, Greece
[c] The Lassonde Faculty of Engineering, York University, 4700 Keele St, Toronto, ON M3J 1P3, Canada

ARTICLE INFO

Keywords:
Shear span
Bond
Yield-penetration
Plastic hinge length
Disturbed region

ABSTRACT

The required confined zone in critical regions of columns and piers undergoing lateral sway during earthquakes is related to the plastic hinge length where inelastic deformation and damage develops. The exact definition of the plastic hinge length stumbles upon several uncertainties, the most critical being that the extent of the inelastic region evolves and spreads with the intensity of lateral displacements. Design codes quantify a reference value for the plastic hinge length, through calibrated empirical relationships that account primarily for the length of the shear span and the diameter of primary reinforcing bars. The latter term reflects the effects of bar yielding penetration in the support of columns. Here a consistent definition of plastic hinge length is pursued analytically with reference to the actual strain state of the reinforcement. Strain penetration extending bilaterally on the reinforcing bars from the critical section towards the column shear span and towards the bar anchorage is evaluated. Considering that bar yielding is synonymous to degradation of interfacial bond between bar and concrete over the yielded area, the field equations of bond are solved explicitly along the column primary reinforcement over the shear span, following the process of gradual crack formation along the member. Boundary effects and important design variables are considered, such as the shear span aspect ratio and the stress-resultants (axial load and flexural moment) carried by the column. Using this solution, the parametric sensitivities of the plastic hinge length are illustrated and compared with other alternatives that have been obtained through experimental calibration. Analytical estimations are also compared with experimental evidence from a number of column specimens tested under axial load and reversed cyclic lateral drift histories reported in the literature.

1. Introduction

The plastic hinge length is used in reinforced concrete (RC) seismic detailing to determine the region where additional confinement requirements apply, but also in performance based seismic design and assessment in order to quantify the deformation capacity of RC columns. It has been studied, quantified and calibrated against tests on isolated column specimens. In the typical test, a cantilever column fixed at the base and carrying a constant axial load is driven to a reversed cyclic lateral load displacement history at the top. Deformation capacity of such members is usually described by the chord rotation that may be sustained by the member prior to loss of its lateral load strength. Contributing to the rotation are the flexural curvature that occurs along the length of the member, as well as the lumped rotation at the critical section resulting from inelastic strain penetration into the support (e.g. footing) as well as inside the shear span. This share of deformation is attributed to reinforcement pullout due to the incompatible length change between the bar and the surrounding concrete.

In columns that do not fail by web crushing, pullout rotation increases gradually with imposed drift, claiming a predominant share of the members' deformation capacity near the ultimate limit state. Column deformation capacity at yielding and ultimate may be computed using a variety of models [1–7]. A stick model is a common point of reference to this purpose: The length of the cantilever L_s corresponds to the shear span of an actual frame member under lateral sway (Fig. 1a); the aspect ratio of the member L_s/h, where h is the cross section depth, quantifies the intensity of shear force demand in the member. Inelastic activity is assumed to occur within an equivalent "plastic hinge length", ℓ_{pl}, whereas the segment of the member outside ℓ_{pl} is assumed to behave elastically. Displacements are calculated from flexural curvatures assuming the curvature distributions of Fig. 1(b,c), which correspond to development of yielding ϕ_y and post-yielding ϕ_u flexural strengths at the support. The plastic rotation developing in the hinge due to flexure is $\theta_{pl}^{f} = (\phi_u - \phi_y)\cdot \ell_{pl}$; similarly, the plastic rotation owing to bar pullout from the support is $\theta_{pl}^{slip} = \theta_u^{slip} - \theta_y^{slip}$ (Fig. 1d); the total plastic rotation is $\theta_{pl} = \theta_{pl}^{f} + \theta_{pl}^{slip}$. The

* Corresponding author at: Dep. of Civil & Environmental Engng, Univ. of Cyprus, 75 Kallipoleos Street, P.O. Box 20537, 1678 Nicosia, Cyprus.
E-mail addresses: kmegal01@ucy.ac.cy (K.G. Megalooikonomou), stastani@civil.duth.gr (S.P. Tastani), pantazo@yorku.ca (S.J. Pantazopoulou).

https://doi.org/10.1016/j.engstruct.2017.11.003
Received 30 December 2016; Received in revised form 25 September 2017; Accepted 6 November 2017

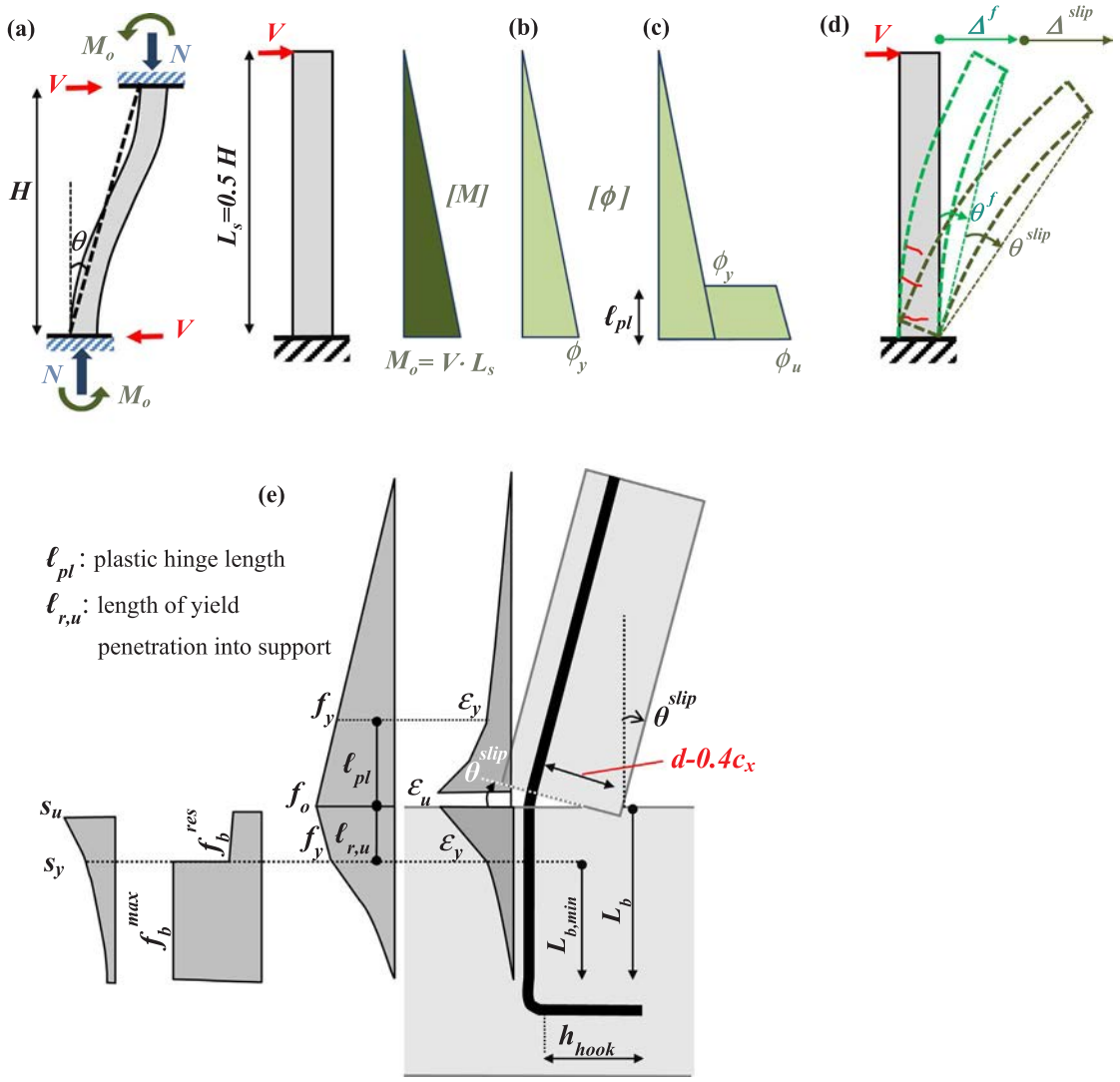

Fig. 1. (a) The stick model for a column under lateral sway. (b)–(c) Distributions of curvature along the column shear span at yielding moment M_y and at flexural strength M_u attained at fixed support ($M_u > M_y$) respectively. (d) Drift components from curvature along shear span (θ^f, Δ^f) and from anchorage slip (θ^{slip}, Δ^{slip}). (e) Bar state of stress/strain (f, ε) along shear span and anchorage of a cantilever column under horizontal loading at the tip. [Note: the bar bond/slip state (f_b, s) is illustrated only for the anchorage.]

corresponding terms are (Fig. 1e) (x is the length counting from the support to the tip of the cantilever column under study):

$$\theta_y^{slip} = \frac{s_y}{(d-0.4c_x)}|_{x=0};\ \theta_u^{slip} = \frac{s_u}{(d-0.4c_x)}|_{x=0};\ s_y \approx \varepsilon_y L_{b,min}/2;\ s_u \approx s_y + 0.5\cdot(\varepsilon_u + \varepsilon_y)\cdot\ell_{r,u};\ L_{b,min} = D_b\cdot f_y/(4f_b^{max});\ \ell_{r,u} = L_b - L_{b,min} \quad (1)$$

where c_x is the depth of compression zone at the critical cross section (here it is assumed to remain constant after yielding) and L_b the total available anchorage length, whereas $L_{b,\min}$ is the minimum required anchorage length to yield a typical bar (diameter: D_b), at a yield stress f_y, considering a uniform bond stress equal to the bond strength of f_b^{max}. Rotation of the critical cross section occurs about the centroid of the compression zone (located at a distance $0.4c_x$ from the extreme compressed fiber based on the equivalent uniform stress block [8]). Parameters s_y and s_u are values of reinforcement pullout slip from the support anchorage at yielding and ultimate (Fig. 1e). Term $\ell_{r,u}$ represents the maximum sustainable penetration of yielding into the anchorage (Fig. 1e); the maximum reinforcement strain, ε_u, that can be supported by the reinforcement at critical cross section (i.e. support) may be estimated assuming that at the extreme, when the anchorage attains its ultimate development capacity the strain distribution along the anchored length is bilinear: $\varepsilon_u = \varepsilon_y + 4(L_b - L_{b,\min})f_b^{res}/(D_b E_{sh})$, where E_{sh} is the hardening modulus of steel and f_b^{res} is the residual bond strength due to cover splitting/delamination. The corresponding maximum and yield flexural curvatures are defined as: $\phi_u = \varepsilon_u/(d - c_x)$ and $\phi_y = \varepsilon_y/(d - c_x)$, whereas the total plastic rotation capacity, θ_{pl}, that may be sustained by the member may be estimated through reverse engineering as [9]:

$$\theta_{pl}^{slip} \approx 0.5\cdot(\phi_u - \phi_y)\cdot\ell_{r,u};\ \theta_{pl}^{f} = (\phi_u - \phi_y)\cdot\underbrace{\left(1 - \frac{M_y}{M_u}\right)}_{a}\cdot L_s \ \Rightarrow\ \theta_{pl} = (\phi_u - \phi_y)\cdot(\underbrace{0.5\cdot\ell_{r,u}}_{(i)} + \underbrace{a\cdot L_s}_{(ii)}) \quad (2a)$$

where in Eq. (2a) index (i) denotes pullout from support and (ii) flexure in the shear span; term α is the strain-hardening ratio of the reinforcement, $a = 1 - M_y/M_u$, defined from cross section analysis at ultimate moment given a simplified stress – strain law for the hardening branch of steel. Introducing the concept of the plastic hinge length, ℓ_{pl}, the plastic rotation capacity from Eq. (2a) is written as:

$$\theta_{pl} \approx (\phi_u - \phi_y)\cdot\ell_{pl} = \phi_{pl}\cdot\ell_{pl};\ \phi_{pl} = \phi_u - \phi_y;\ \ell_{pl} = 0.5\cdot\ell_{r,u} + \alpha\cdot L_s \quad (2b)$$

Empirical equations for the plastic hinge which have prevailed in

design Codes [5,10] and in research [1,11–15] have the form of Eqs. (3a) and (3b) respectively:

$$\ell_{pl} = 0.08L_s + 0.022 \cdot D_b \cdot f_y \tag{3a}$$

$$\ell_{pl} = 0.1L_s + 0.17 \cdot h + 0.24 \cdot D_b \cdot f_y / \sqrt{f_c'} \tag{3b}$$

with h being the column sectional depth and f_c' the concrete compressive strength. (For example, 0.08 and 0.1 are common values for the strain hardening ratio α of common reinforcement, whereas the term proportional to the bar diameter D_b, which represents the strain penetration length within the anchorage, is intended for well-designed anchorages that can easily support strain penetration lengths of $10 \sim 20D_b$).

In the presence of high axial load N, the required confined length ℓ_c is obtained from the basic value of ℓ_{pl} by adding terms to account for the tension shift in the shear span of a member and the increased demands for confinement [16] (γ_c in Eq. (3c) is a strength–reduction factor):

$$\ell_c = \ell_{pl} + 0.5h; \ \frac{\ell_c}{h} = 1 + 2.8 \cdot \frac{N}{\gamma_c \cdot f_c' A_g} \tag{3c}$$

Bae and Bayrak [15] proposed an alternative expression of ℓ_{pl}, derived from correlation with column experiments under various axial load levels, recognizing explicitly the important variables that control ℓ_{pl}:

$$\frac{\ell_{pl}}{h} = \left[0.3 \cdot \left(\frac{N}{N_o}\right) + 3 \cdot \left(\frac{A_s}{A_g}\right) - 0.1\right] \cdot \left(\frac{L_s}{h}\right) + 0.25 \geqslant 0.25 \tag{3d}$$

where h is the column depth, N is the applied axial load, $N_o = 0.85f_c'(A_g - A_{s,tot}) + f_y A_{s,tot}$, f_c' is the concrete compressive strength, A_s is the area of tension reinforcement, $A_{s,tot}$ is the total reinforcement area, and A_g the gross area of concrete section.

A significant limitation of the theoretical definition of ℓ_{pl}, as given by Eq. (2b), is that it breaks down if the moment-curvature response of the member is elastic – perfectly plastic (i.e., $M_y = M_u$, $a = 0$), leading to a rather small plastic hinge length. This is counter-intuitive when considering that a necessary accessory to rebar yielding is the localized loss of bond. Thus point-yielding of column reinforcement with no penetration to adjacent areas is physically impossible. In practical applications, to resolve the indeterminacy caused in Eq. (2b) due to elastoplasticity, ℓ_{pl} is taken as $0.5\,h$, or Eqs. (3a), (3b) are used directly without reference to the underlying physical model. The apparent inconsistency inherent in the theoretical definition of ℓ_{pl} is partly responsible for the poor correlation of the estimated deformation capacity of flexure-dominated columns with results from experimental databases [17,18]. An alternative is to explicitly solve for the plastic hinge length by establishing and solving the field equations of bond along the principal reinforcement (in the shear span) of the deformed member under lateral sway, with particular emphasis on the part of the reinforcement that is strained beyond the limit of yielding into the hardening range.

This modelling approach is pursued in the present paper. A unidirectional model of bond is considered as a basis for the evaluation of the longitudinal strain distribution of the primary reinforcement of the column [19]. The processes of sequential crack formation due to tension stiffening, and the subsequent crack opening are explicitly considered. In the analysis, large localized slip magnitudes lead to bond degradation that is accompanied by spread of inelastic strains both in the shear span and in the anchorage. Although several solutions that refer to the problem of force development along the anchorage have been proposed, yet the problem of strain penetration in the anchorage has received limited attention from researchers [19,20]. On the other hand, the problem of strain penetration in the shear span of the member has not been addressed explicitly yet and therefore it represents the main scope of the present paper. In this study, strain distributions in the shear span and in the bar anchorage are evaluated using a step by step calculation algorithm; controlling variable is the tension strain magnitude at the critical cross section (support of the cantilever). Through this process disturbed regions are identified in the shear span, where bar strains are controlled by bond development rather than the "plane-sections" assumption. Using this approach, the parametric sensitivities of the plastic hinge length are illustrated and compared with the other alternatives summarized in the preceding obtained from experimental calibration. Application of the analytical procedure for estimating the plastic hinge length is demonstrated through comparison with column specimens tested under axial load and reversed cyclic lateral drift histories reported in the literature.

2. Governing equations of bond-slip behavior in concrete

The basic equations that describe force transfer lengthwise from a bar to the surrounding concrete cover through bond are derived from force equilibrium established on an elementary bar segment of length dx [21,22]:

$$df/dx = (-4/D_b) \cdot f_b \tag{4a}$$

where f is the axial stress of the bar; D_b is the bar diameter; f_b is the local bond stress. Furthermore, compatibility between the relative translation of the bar with respect to the surrounding concrete, (i.e., slip = s), the axial bar strain ε, and concrete strain ε_c over dx requires that [21,22]:

$$ds/dx = -(\varepsilon - \varepsilon_c) \cong \varepsilon \tag{4b}$$

For normal concrete, term ε_c is neglected as its tensile value cannot exceed the cracking limit ($\varepsilon_{c,cr} \approx 0.00015$) which is well below the other terms of Eq. (4b). Bond stress and slip, and bar stress and strain are related through the interface and material constitutive relationships, $f_b = f_b(s)$ and $f = f(\varepsilon)$. Solution of Eq. (4) is possible though exact integration, resulting in closed-form expressions for the state of stress and strain along the anchorage, through pertinent selection of simple models for the material laws (e.g. piecewise linear relations). This approach has a clear advantage over the numerical solution alternative in that it enables transparent insight into the role of the various design parameters on the behavior of bar anchorages and/or lap splices.

Here the reinforcing bar stress-strain relationship is considered elastoplastic with hardening (representing conventional steel reinforcement, Fig. 2a). Without loss of generality, and to facilitate derivation of closed-form solutions, a linear elastic, perfectly plastic local bond-slip relationship with residual bond is assumed (Fig. 2b). The plateau in the local bond-slip law implies sustained bond strength. This feature is not always manifested in the test data; to be measured it requires redundancy in the anchorage (i.e., availability of longer anchorages to enable force redistribution towards the healthy part of the anchorage before failure). In the assumed law the end of the plateau is marked by abrupt loss of bond strength to the residual value f_b^{res}. (Note that f_b^{res} is taken nonzero only in the case of ribbed steel bars, but not for smooth steel bars.) The last branch represents the residual friction between the concrete cover and the steel bar after failure of the rib interlocking mechanism.

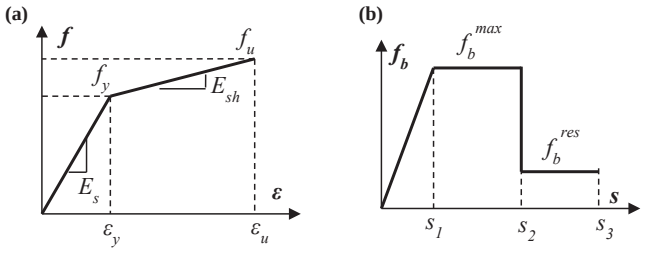

Fig. 2. (a) Assumed stress-strain law of steel reinforcing bar. (b) Assumed local bond-slip law.

Strain penetration occurs in the bars beyond the critical section due to the degradation of bond beyond slip limit s_2, that marks the end of the plateau in the local bond-slip law. This stage may be attained in different ways along a bar: (a) for yielding to occur, i.e. constant bar stress ($=f_y$, $df/dx = 0$) for a range of values of bar strain $\varepsilon > \varepsilon_y$, bond should be eliminated ($f_b^{res} = 0$); if f_b^{res} is nonzero, then a yielded bar will demonstrate a commensurate amount of strain hardening. (b) If the bar is elastic (e.g. FRP bar), then for large strain levels bar slip values are increased to levels beyond s_2 (Fig. 2b): this is marked by debonding and cover splitting of the loaded end of anchorage thereby limiting the development capacity of the reinforcement.

Strain penetration of yielding over a bar anchorage has received some attention, especially with regards to its contribution to rotation capacity of structural members [19,20,23,24]. But the implications resulting from spreading of inelastic strains in the shear span of a structural member on the development capacity of reinforcement and on member behavior have not yet been described with reference to the mechanics of bond.

Consider a reinforcing bar that spans the deformable length of a structural column, anchored in its footing. An important difference may be traced in the state of stress occurring in the two regions along the bar: within the anchorage stress is controlled by the mechanics of bond, as described by the field equations (Eq. (4)). On the other hand, within the shear span, it is the prevailing notion that bar stress is controlled by flexural theory; i.e. the requirement of plane sections remaining plane at any cross section relates bar strains to flexural moment and axial load through cross sectional equilibrium. This however can be incompatible with the requirements of Eq. (4). The concept of tension stiffening is used in order to settle this potential conflict between the two antagonistic mechanisms for control of reinforcement strains: a certain nontrivial length ℓ_{Do} is needed, measured from the face of the crack toward the un-cracked part of the member until bar strain compatibility with the surrounding concrete cover may be claimed. Thus, the field equations of bond control the segment ℓ_{Do}, whereas the classical theory of bending controls the remaining length. The region over the shear span of a flexural member where bar stresses are controlled by the mechanics of bond (Eq. (4)) rather than the mechanics of flexure, is referred to hereon as a “disturbed” region, thereby assigning to this length an alternative interpretation from that used to explain shear dominated response in frame members [25]. At the same time this alternative significance of the disturbed region underscores the interaction between bond and shear strength [26]. Clearly, as flexural cracking propagates the disturbed zone extends and may spread over the entire length of the member.

3. Disturbed region on shear span of a flexural member

It was mentioned earlier that spread of inelastic strains occurs on both sides of a critical section (i.e. at the base of a column). The process of inelastic strain penetration in the anchorage of a reinforcing bar has already been demonstrated in Tastani and Pantazopoulou [19,20]. This section is dedicated to solving the same problem in the other side of the critical section, that is, over the disturbed region along the shear span of a column. Here the problem is different from that of the anchorage in the type of boundary conditions that may be enforced for the governing differential equation (Eq. (4)). The bond-slip law has the same multilinear envelope as in the case of an anchorage, however the bond strength value, f_b^{max}, is a function of the available transverse reinforcement.

3.1. Evaluation of disturbed length on crack initiation

For the stage prior to the occurrence of flexural cracking along the length of the member, the bar strain is estimated from the flexural analysis of the un-cracked column cross section (i.e. from the moment-curvature analysis, Fig. 3a):

$$\varepsilon_{fl}(x) = \phi(x)\cdot y_{s,na}^{gr} \tag{5a}$$

This is expressed explicitly as:

$$\varepsilon_{fl} = \frac{M(x)}{E_c\cdot I_g}\cdot y_{cg} - \frac{N}{E_c\cdot A_g};\quad y_{cg} = \frac{h}{2} - C_{cov} - 0.5D_b;\ y_{s,na}^{gr} = y_{cg} - \frac{N}{M}\cdot\frac{I_g}{A_g} \tag{5b}$$

where $M(x)$, N (+ for compression) and $\phi(x)$ are the flexural moment, axial load and flexural curvature acting on the member section at distance x from the support, E_c is the elastic modulus of concrete, I_g and A_g are the moment of inertia and the uncracked cross section area, h is the section height and C_{cov} is the clear cover (Fig. 3a). Parameters $y_{c,g}$ and $y_{s,na}^{gr}$ are the distances of the centroid of tension reinforcement to the centroid of the uncracked cross-section and to the neutral axis location, respectively (Fig. 3a). The distance to the neutral axis changes significantly from the initial linear elastic state $y_{s,na}^{gr}$, to the cracked state of a cross section, $y_{s,na}^{cr}$. Generally, the position of the neutral axis may be estimated from equilibrium requirements, both in the uncracked cross sections as well as at the crack locations assuming “plane sections remain plane”. From the flexural analysis perspective, when the flexural moment $M(x)$ exceeds the cracking moment, M_{cr} [$=(f_{ct} + N/A_g) \times I_g/(0.5h)$, where f_{ct} the tensile strength of concrete, N is the axial load –compression positive-, A_g the cross section area of column, I_g the gross moment of inertia and h the cross section height] even by a small amount, then the member may be considered cracked in the neighborhood of x. Although a large region may satisfy this definition, however, cracks i occur at discrete locations $x_{cr,i}$. Thus, if an analysis of the cracked cross section is available (based on plane section hypothesis), the tension reinforcement strains $\varepsilon(x_{cr,i})$ that occur in the crack locations may be calculated from:

$$\varepsilon(x_{cr,i}) = \phi(x_{cr,i})\cdot y_{s,na}^{cr} \tag{6}$$

In the segment between successive cracks where moment exceeds the cracking value, bar strains cannot be estimated from flexural analysis as prescribed by Eq. (6). Owing to reinforcement slip, the degree of strain compatibility between steel and concrete in these locations is not well understood, as would be required by the “plane-sections remain plane” assumption, nor can the concrete be considered inert as would happen in a fully cracked tension zone. Because it takes some distance from a crack location before the reinforcement may fully engage its concrete cover in tension again so as to satisfy the conditions of strain compatibility, Eq. (6) is invalid even in the region immediately adjacent to the last flexural crack in the shear span, although the flexural moment is below the cracking limit in that region. Bar strain over cracked segments of the member may be estimated from solution of Eq. (4). To address all the possible exceptions to the validity of the flexural requirement stated by Eqs. (5) and (6), here the term “undisturbed” is used as a qualifier to “un-cracked” in order to refer to sections that also satisfy “the plane sections remaining plane” compatibility requirement. As a corollary, where strains are obtained from solution of the bond equation, the region is “disturbed”.

The flexural moment at a distance x from the face of the support is estimated with reference to the flexural moment at the support, M_o (ε_o is the bar tension strain at $x = 0$, Fig. 3b):

$$M(x) = M_o\cdot(1 - x/L_s) \tag{7}$$

As the sequence of crack formation is critical for the occurrence of disturbed regions and for the problem of strain penetration that will be subsequently addressed, in the present discussion the static problem represented by Eq. (7) will be solved for a gradually increasing value of the support moment, M_o. It is assumed that the characteristic flexural resistance curve (moment-curvature) of any cross section along the shear span (i.e. the moment – curvature and moment – bar strain diagram) is available from classical flexural analysis (plane-sections) for the entire range of response.

For a member with continuous primary reinforcement over the shear span, L_s, the moment distribution that follows Eq. (7) will cause

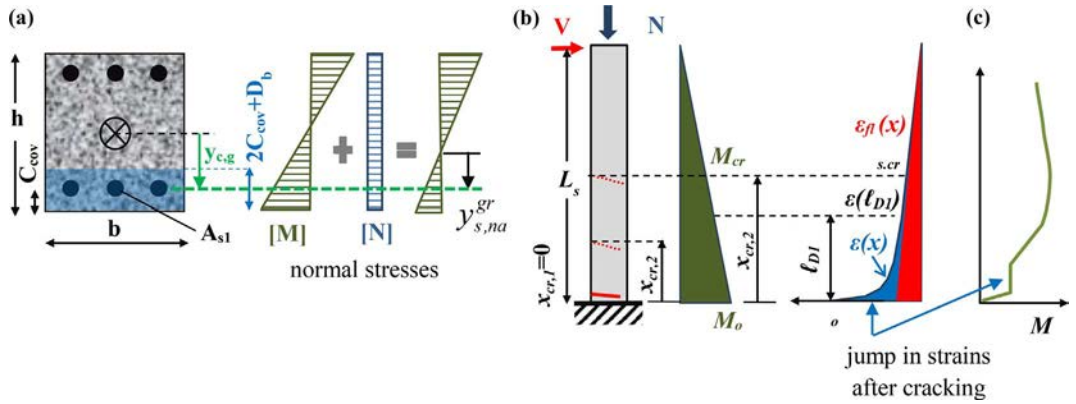

Fig. 3. Definition of terms: (a) Cross sectional flexural analysis. (b) Bar strain distribution along the shear span L_s: stage prior to cracking (red); response into the disturbed region ℓ_{D1} (blue). (c) Moment - bar strain diagram. (For interpretation of the references to colour in this figure legend, the reader is referred to the web version of this article.)

first cracking at the face of the support ($x_{cr,1} = 0$, Fig. 3b). Upon cracking of the tension zone the bar strain experiences a significant jump to maintain equilibrium (Fig. 3c). For example, if the cracked section stiffness is about 1/3 of the uncracked value, the bar strain at the critical section is expected to increase threefold by the mere occurrence of the crack even though the moment change from the uncracked to the cracked stage may be imperceptible. Thus suddenly the whole region adjacent to the cracked location becomes "disturbed". Over the length of the disturbed region, ℓ_{D1} (Fig. 3b) the reinforcement strain is described by the solution of the bond equation [19,20]:

$$\varepsilon(x) = C_1 \cdot e^{-\omega x} + C_2 \cdot e^{\omega x}, \text{ where, } \omega = [4 f_b^{max}/(E_s \cdot D_b \cdot s_1)]^{0.5} \quad (8)$$

The solution of Eq. (8) is valid provided bond is in the elastic range (ascending branch in the bond slip law, Fig. 2b). Before the creation of a second crack, the following conditions characterize the end of the disturbed region at $x = \ell_{D1}$:

(a) the slope of the bar strain distribution, $\psi = d\varepsilon(x)/dx$, obtained from differentiation of Eq. (8), matches that of the strain diagram as would be obtained from Eqs. (5b) and (7):

$$\psi = d\varepsilon(x)/dx \rightarrow \omega \cdot (-C_1 \cdot e^{-\omega \ell_{D1}} + C_2 \cdot e^{\omega \ell_{D1}}) = -\varepsilon^o_{el} \cdot 1/L_s \text{ where } \varepsilon^o_{el} = (M_o \cdot y_{cg})/(E_c \cdot I_g) \quad (9a)$$

(b) the bar strain $\varepsilon(\ell_{D1})$ satisfies both Eqs. (5b) and (8):

$$\varepsilon(\ell_{D1}) = C_1 \cdot e^{-\omega \ell_{D1}} + C_2 \cdot e^{\omega \ell_{D1}} = \varepsilon^o_{el} \cdot (1 - \ell_{D1}/L_s) - N/(E_c \cdot A_g) \quad (9b)$$

Given the axial load N and the bar strain at the support $\varepsilon(x = 0) = \varepsilon_o$ the corresponding moment M_o is obtained from the moment-curvature analysis of the cracked section. A boundary condition of Eq. (8) is,

$$\varepsilon(x = 0) = C_1 + C_2 = \varepsilon_o \quad (9c)$$

Unknowns of the system of Eq. (9) are, the disturbed length ℓ_{D1} (Fig. 3b), and the coefficients C_1 and C_2. In an algorithm developed to solve Eq. (9) numerically, the controlling parameter is ε_o; required input includes the axial load, N, shear span L_s, the bond-slip characteristic property ω (Eq. (8)), and the member material and cross sectional properties. Coefficients C_1, C_2 are obtained from (9a) and (9b):

$$C_{1,2} = 0.5 \cdot e^{\beta \cdot \omega \ell_{D1}} \left[\varepsilon^o_{el} \cdot \left(1 - \frac{\ell_{D1}}{L_s} + \frac{\beta}{\omega L_s} \right) - N/(E_c \cdot A_g) \right], \text{ where } \beta = 1 \text{ for } C_1, \text{ and } \beta = -1 \text{ for } C_2 \quad (10)$$

The value of ℓ_{D1} is determined by solving Eq. (9c) after substitution of C_1, C_2.

3.2. Formation of additional flexural cracks in the shear span

Increasing the reinforcement strain value at the critical section, ε_o, corresponds to a higher flexural moment M_o at the support. Based on Eq. (7), the flexural moments exceed the cracking moment up to a distance x_{cr} from the support: $x_{cr} = L_s \cdot (1 - M_{cr}/M_o)$. But the position of the next crack is not necessarily at x_{cr}; rather, it is controlled by tension stiffening of the reinforcement.

(a) To determine if the next crack forms within ℓ_{D1}, (Fig. 3b) the force transferred through bond to the concrete cover (i.e. $E_s A_{s1}[\varepsilon_o - \varepsilon(x)]$) is compared with the tensile resistance of the effective area of concrete cover engaged in tension (i.e. $f_{ct} A_{c.eff}$, [27])

$$[(E_s \cdot A_{s1})/(f_{ct} \cdot A_{c.eff})] \cdot [\varepsilon_o - \varepsilon(x)] \geqslant 1, \; A_{c.eff} = b \cdot (2C_{cov} + D_b) - A_{s1} \quad (11)$$

where A_{s1} is the area of the tensile reinforcement, $A_{c.eff}$ is the area of concrete effectively engaged in tension (shaded area around A_{s1} in Fig. 3a), f_{ct} is the tensile concrete strength, and b is the width of the section of the column (Fig. 3a). The lowest value of $x = x_{cr,2} < \ell_{D1}$ that satisfies Eq. (11) determines the location of the next crack; otherwise no further cracking is possible within ℓ_{D1} as long as the reinforcement remains elastic.

(b) Alternatively, the next possible crack location, $x_{cr,2} \geq \ell_{D1}$ in the undisturbed region (Fig. 3b) is also evaluated from Eq. (5b) (here, $\varepsilon_{s.cr} = \varepsilon_{c.cr} \times y_{cg}/(0.5h)$ is the strain at the level of reinforcement–Fig. 3a- when the concrete strain on the tension surface of the column is equal to the cracking limit $\varepsilon_{c.cr} = f_{ct}/E_c$, in the order of 0.00015):

$$\varepsilon(x) = \varepsilon^o_{el}(1 - x/L_s) - N/(E_c \cdot A_g) = \varepsilon_{s.cr} \Rightarrow x_{cr,2} = L_s \cdot [1 - \varepsilon_{s.cr}/\varepsilon^o_{el} - N/(E_c A_g \varepsilon^o_{el})] \quad (12)$$

Slip in the disturbed region is obtained from integration of bar strains (from $x = 0$ to $x = \ell_{D1}$).

$$s(x) = \frac{1}{\omega}(C_1 \cdot e^{-\omega x} - C_2 \cdot e^{\omega x}) + C \quad (13)$$

The constant of integration, C is obtained from the requirement of compatibility of strains in the concrete and reinforcement at the end of the disturbed zone, $x = \ell_{D1}$ where the local slip is zero ($s(\ell_{D1}) = 0$).

After localization of the second crack at $x_{cr,2}$, the next step of the solution is the determination of the new disturbed region ℓ_{D2} (along with the updated values of the constants C_1, C_2). Term ℓ_{D2} initiates from the crack location $x_{cr,2}$ and extends towards the span until the requirements of slope coincidence and continuity are reached, at coordinate $x_{cr,2} + \ell_{D2}$ in Eqs. (9a) and (9b) (Fig. 4a). In using the closed form expression of Eq. (8), the value of x is substituted by the value x-

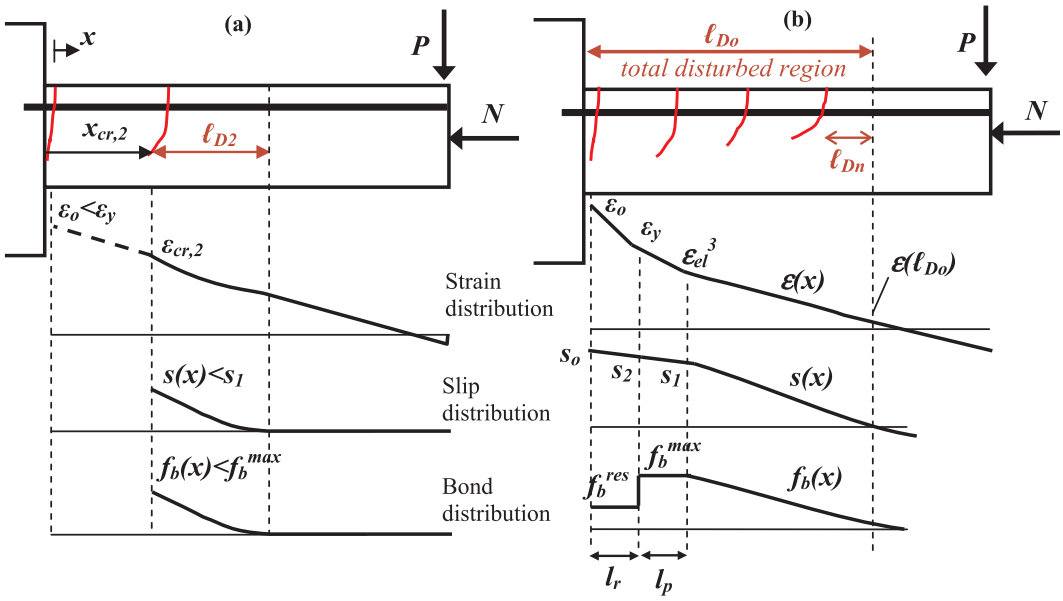

Fig. 4. (a) Disturbed region ℓ_{D2} after formation of the 2nd crack. (b) Total disturbed region ℓ_{Do} after stabilization of cracking.

$x_{cr,2}$; this solution is valid for x ⊆ $[x_{cr,2}, x_{cr,2} + \ell_{D2}]$). The bar strain $\varepsilon_{cr,2}$ at the location of the second crack (Fig. 4a) is the outcome of the flexural analysis of the cracked section and corresponds to the moment at that location according to Eq. (7) for $x = x_{cr,2}$. In the search of the new disturbed region, an additional requirement is that slip at the location $x_{cr,2}$ should not exceed the limit s_1 in Eq. (13) (where x is substituted by x-$x_{cr,2}$), securing that bond is still elastic inside ℓ_{D2} (Fig. 4a).

This process is repeated following the gradual increase in the value of bar strain ε_o at the support, until no additional primary cracks can be identified. This point corresponds to stabilization of cracking, and it generally occurs at a strain value in the critical section that is less than the strain at yielding, $\varepsilon_o^{stbl} < \varepsilon_y$. From this stage and until failure of the structural member, for the sake of simplicity of the mathematical problem, the so called *total disturbed region* ℓ_{Do} is defined as the total distance measured from the support to the end of the disturbed region of the last (and remotest) crack that was formed prior to stabilization, ℓ_{Dn} (Fig. 4b). Since bond development controls the total disturbed region, from that point onwards the field equations (Eq. (4)) are solved in ℓ_{Do} ignoring the presence of intermediate discrete cracks or the flexural moment requirements, since the "plane sections" assumption is not valid anywhere over this entire region; upon further increase of the bar strain at the support, the ℓ_{Do} length may increase further as the disturbed zone penetrates towards the tip of the cantilever column.

Following cracking stabilization and beyond yielding of the steel bar ($\varepsilon_o > \varepsilon_y$), the yielded segment of the disturbed region undergoes simultaneous degradation of bond. Thus, of the total length ℓ_{Do}, there is a segment l_r where yielding penetrates and spreads with increasing value of ε_o (Fig. 4b). Owing to bar yielding, bar strains increase over l_r without a commensurate increase of stress: this means that bond must have degraded to zero as a consequence of Eq. (4a), since $df/dx = 0$ and thus $f_b = 0$. This segment may be considered debonded. Even if the yield-plateau is neglected, and the bar stress-strain diagram is considered bilinear with some hardening (Fig. 2a), it is clear that the small hardening slope may only be supported by the residual bond strength – in other words in order for a bar to yield, it must have slipped beyond the limit s_2 in the bond-slip law (Fig. 2b). Limit s_2 is not an intrinsic property of the bar–concrete interface as it is generally assumed by Design Codes [28], but rather, it depends on the available bonded length [19].

Solution for the distributions of strain, slip and the state of bond over the disturbed region ℓ_{Do} of the shear span of a column under lateral sway follows that obtained when considering yield penetration in a bar anchorage [19]. Here, the disturbed region ℓ_{Do} comprises the sequence of the following segments (Fig. 4b): the yield penetration length l_r (immediately adjacent to the support), the bond plastification length l_p (i.e. the length where the bar is elastic but bond is constant and equal to the value at the plateau of the bond slip law, f_b^{max}); Bar axial stress and bond stress are elastic in the tail length of the disturbed region. The solution of the bond equations for the different segments is given below:

$$\text{For } 0 \leqslant x \leqslant l_r\text{: } \varepsilon(x) = \varepsilon_o - \frac{4f_b^{res}}{E_{sh}D_b}x;\ f_b(x) = f_b^{res} \tag{14a}$$

$$s(x) = s_2 + 0.5(l_r - x)[\varepsilon(x) + \varepsilon_y] \rightarrow x = 0\text{: } s_o = s_2 + 0.5l_r\cdot(\varepsilon_o + \varepsilon_y) \tag{14b}$$

$$\text{For } l_r \leqslant x \leqslant l_r + l_p\text{: } \varepsilon(x) = \varepsilon_y - \frac{4f_b^{max}}{E_sD_b}(x - l_r);\ f_b(x) = f_b^{max} \tag{15a}$$

$$s(x) = s_1 + 0.5(l_r + l_p - x)[\varepsilon(x) + \varepsilon_{el}^3] \rightarrow x = l_r\text{: } s_2 = s_1 + 0.5l_p\cdot(\varepsilon_y + \varepsilon_{el}^3) \tag{15b}$$

$$\varepsilon_{el}^3 = \varepsilon_y - \frac{4f_b^{max}}{E_sD_b}l_p \tag{15c}$$

$$\text{For } l_r + l_p \leqslant x \leqslant \ell_{Do}\text{: } \varepsilon(x) = C_{1t}\cdot e^{-\omega(x-l_p-l_r)} + C_{2t}\cdot e^{\omega(x-l_p-l_r)};\quad f_b(x) = \frac{f_b^{max}}{s_1}\cdot s(x) \tag{16a}$$

$$s(x) = \frac{1}{\omega}(C_{1t}\cdot e^{-\omega(x-l_p-l_r)} - C_{2t}\cdot e^{\omega(x-l_p-l_r)}) + C_t \tag{16b}$$

Unknowns ℓ_{Do}, C_{1t}, C_{2t} and the constant of integration C_t are obtained from boundary conditions at $x = \ell_{Do}$ (namely slope and strain continuity and slip compatibility - zero relative displacement) between strain distributions obtained from the bond development equation and from flexural analysis. Therefore reinforcement slip is: at $x = l_r + l_p$, $s(x) = s_1$; at $x = \ell_{Do}$, $s(\ell_{Do}) = 0$ (see Fig. 4b). The following system of boundary conditions is therefore established:

(a) Slope continuity of the strain distributions at $x = \ell_{Do}$:

$$\omega\cdot(-C_{1t}\cdot e^{-\omega(\ell_{Do}-l_r-l_p)} + C_{2t}\cdot e^{\omega(\ell_{Do}-l_r-l_p)}) = -\varepsilon_{el}^o\cdot 1/L_s,\ \varepsilon_{el}^o = (M_o\cdot y_{cg})/(E_c\cdot I_g) \tag{17a}$$

(b) Continuity of strains at $x = \ell_{Do}$:

$$\varepsilon(\ell_{Do}) = C_{1t}\cdot e^{-\omega(\ell_{Do}-l_r-l_p)} + C_{2t}\cdot e^{\omega(\ell_{Do}-l_r-l_p)} = \varepsilon_{el}^{o}\cdot(1-\ell_{Do}/L_s)-N/(E_c\cdot A_g) \quad (17b)$$

(c) Continuity of slip at $x = l_r + l_p$:

$$s\cdot(l_r + l_p) = \frac{1}{\omega}(C_{1t}-C_{2t}) + C_t = s_1 \quad (17c)$$

(d) Continuity of strain at $x = l_r + l_p$:

$$\varepsilon\cdot(l_r + l_p) = C_{1t} + C_{2t} = \varepsilon_{el}^{3} \quad (17d)$$

The length of yield penetration l_r (Eq. (18)) may be estimated considering the continuity of strain at $x = l_r$ (in Eq. (14a)).

$$l_r = (\varepsilon_o-\varepsilon_y)\cdot\frac{E_{sh}D_b}{4f_b^{res}} \quad (18)$$

Eq. (18) for the yield penetration length (which defines the plastic hinge length) has two interesting implications: first, it is a strain-based criterion for the spread of yielding in the shear span, as opposed to the stress-based definition given by Eq. (2b); there the coefficient a refers to the flexural overstrength normalized by the yielding moment. A second more subtle point is the observation that the plastic hinge length is influenced by several parameters indirectly, through the determining effect that these have on f_b^{res}. For example the presence of axial load on a member that undergoes cyclic displacement reversals weakens the cover over a larger portion of the shear span length leading to cover delamination due to excessive compressive strains; upon reversal of load, the crushed cover cannot support significant bond action for the reinforcement when it is stressed in tension, leading to a reduced value of f_b^{res}, which in turn causes increased penetration depth for columns carrying a higher axial load; this is consistent with experimental reports [15,16,30].

The following algorithm (Fig. 5) is established in order to define the locations of primary cracks and bar strain, slip and bond distribution along the shear span L_s of a laterally loaded reinforced concrete column as well as the yield penetration length:

Initial Data: Using standard section analysis obtain *M-ϕ* and *M-ε* diagrams (or better a unified diagram M-*ϕ*-*ε*) given *N* for the typical section of the reinforced concrete column studied.
1st Step: Select value of bar strain, $\varepsilon_o^{(1)} = \varepsilon_o$, after crack formation at the support (Eq. (5), (7)).
2nd Step: Find the corresponding moment, M_o at the support, from moment-bar strain diagram. Solve for the length of the disturbed region ℓ_{D1} emanating from the first crack (Eqs. 8–10).
3rd Step: Increase strain at critical section to $\varepsilon_o^{(2)} = \varepsilon_o^{(1)} + \Delta\varepsilon_o$. Find the location $x_{cr,2}$ of the second crack. Check if second crack will occur: (a) inside ℓ_{D1} according to Eq. (11), or (b) in the undisturbed region L_s- ℓ_{D1}, according to Eq. (12).
4th Step: (a) If next crack forms within ℓ_{D1}, repeat Step 3 for $\varepsilon_o^{(3)} = \varepsilon_o^{(2)} + \Delta\varepsilon_o$. (b) Otherwise, find the new disturbed region ℓ_{D2} that extends beyond $x_{cr,2}$.
5th Step: Find total disturbed length, $\ell_{Do} = x_{cr,2} + \ell_{D2}$.
6th Step: Solve for $\varepsilon(x)$, $s(x)$, $f(x)$, $f_b(x)$ for $x_{cr,2} \le x \le \ell_{Do}$ from Eqs. ((8), (9), (10), (13)) (Fig. 4a). In this phase of the solution and up to stabilization of cracking elastic bond is assumed in ℓ_{D2} (Fig. 4a). Thus the distributions can be described by the Eq. (16) after substituting $l_r = 0$ and $l_p = 0$. For L_s-ℓ_{Do} < x < L_s, (elastic column) Eq. ((5), (7)) are used.
7th Step: Repeat steps 2–6 for $\varepsilon_o^{(i)} = \varepsilon_o^{(i-1)} + \Delta\varepsilon_o$ until stabilization of cracking (i.e., no more primary cracks can develop: $\varepsilon_o^{stbl} = \varepsilon_o^{(i)}$). Final length of disturbed zone is obtained from the n^{th} increment using this procedure: $\ell_{Do} = x_{cr,n} + \ell_{Dn}$.
8th Step: Increase $\varepsilon_o^{(i)} = \varepsilon_o^{(i-1)} + \Delta\varepsilon_o > \varepsilon_o^{stbl}$. Solve for one continuous disturbed region $\ell_{Do} \ge x_{cr,n} + \ell_{Dn}$ allowing for bond plastification and debonding as well as bar yielding (anchorage solution) up to either (a) ε_o exhausting the ultimate strain of the *M-ε* diagram, or (b) ℓ_{Do} exceeding the available development length of the bar in the shear span, taken here as ($L_s + h_{hook}$), where h_{hook} (Fig. 1e) refers to the bent length of a hooked anchorage (according with [28] the contribution of a hook to the strength of an anchored bar is $50A_bf_b^{max}$, which corresponds to an additional anchored length, $\Delta L_b = h_{hook} = 12.5D_b$). If (b) controls, continue beyond that point for higher strains using the anchorage solution [19] for the entire length ℓ_{Do}.
9th Step: The last converged value of l_r in the shear span (Fig. 4b) is added to the corresponding yield penetration length into the anchorage [19] resulting in the definition of the total plastic hinge

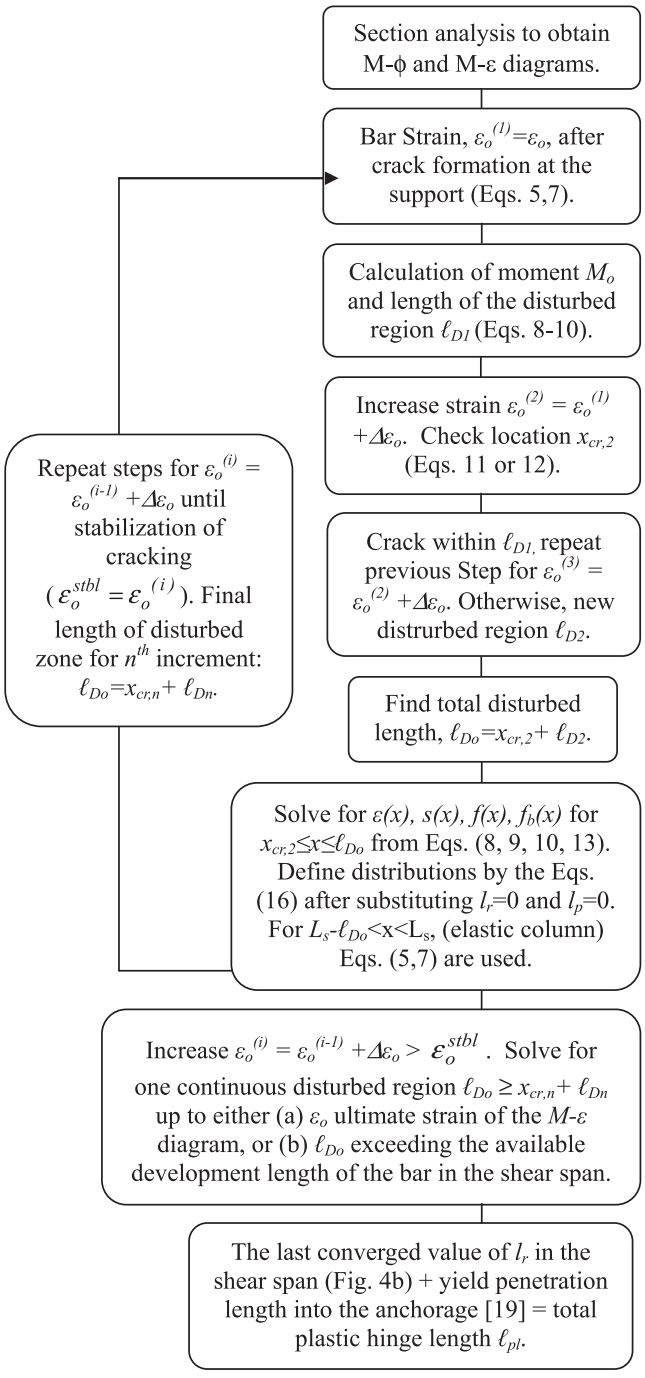

Fig. 5. Flow-chart of the established algorithm for the definition of the bond state in the disturbed region of the shear span as well as of the plastic hinge length.

length ℓ_{pl}.

4. Results

In the context of the present paper, the length of plastic hinge is by definition the length of yield penetration (thus $\ell_{pl} = l_r$), occurring from the critical section towards both the shear span and the anchorage; physically it refers to the extent of the region where nonlinear reinforcing strains occur, and it may be used to calculate the inelastic rotation capacity of the column. The solution algorithm developed is applied in this section in order to establish the parametric sensitivities of the estimated plastic hinge to the important design parameters. It is also used to correlate the behavior of the plastic hinge spread in three published column tests that were conducted to illustrate the effect of axial load on the length of the plastic hinge region [29,30].

4.1. Application examples

The three column experiments studied in the paper are specimens U3 [29], S17-3UT and S24-4UT [30]. Column specimens were tested as cantilevers, simulating half a clear column length under lateral sway such as would occur during an earthquake with cross section detailing as shown in Fig. 6a. Column U3 is analyzed in detail and results are summarized in Table 1, whereas results of S17-3UT and S24-4UT are directly included in Table 1 for easy correlation.

4.1.1. Column U3 [29]

The specimen had a 350 mm square cross section reinforced with eight evenly distributed longitudinal reinforcing bars of D_b = 25 mm and stirrups of $D_{b,st}$ = 10 mm spaced at 75 mm o.c. (on centers) and clear cover C_{cov} = 32.5 mm (i.e., d = 350–45 = 305 mm), see Fig. 6a. Concrete strength was f_c' = 34.8 MPa. Longitudinal steel yielding strength was 430 MPa with a 5% hardening. Stirrup yield strength was 470 MPa.

Column shear span was L_s = 1.0 m and the axial load ratio [$\nu = N/(f_c' bd)$] was 0.16. Fig. 6b plots the unified M-ϕ-ε relationship obtained for this axial load using fiber section analysis with the modified Kent & Park model for confined concrete [31]; a Hognestad-type parabola was used to model the compression stress-strain response of unconfined concrete [32]. A bilinear stress-strain curve with 5% hardening was used to model longitudinal reinforcement (Fig. 2a). Bond strength was taken equal to $f_b^{max} = 1.25\sqrt{f_c'}$ (7.4 MPa) for the anchorage (anchorage with hook with equivalent straight length of L_b = 812 mm [28]). For the shear span the bond strength is calculated using a frictional model [33] that accounts for separate contributions of the cover concrete and stirrups according to:

$$f_b^{max} = \frac{2\mu_{fr}}{\pi D_b}\left(2C_{cov} \cdot f_{ct} + 0.33\frac{A_{st} f_{y,st}}{N_b \cdot S}\right) \tag{19}$$

where N_b is the number of tension bars (or pairs of tension spliced bars if reinforcement is spliced) laterally restrained by the transverse pressure exerted in the form of confinement by the stirrups, C_{cov} is the clear concrete cover, A_{st} is the area of stirrup legs enclosing the N_b bars (i.e., the total area of legs crossing the splitting plane), S is the stirrup spacing along the member length, μ_{fr} is coefficient of friction, f_{ct} is the concrete tensile strength and $f_{y,st}$ is the yielding strength of stirrups. Therefore the maximum bond strength for the shear span is 7.2 MPa when considering the contribution of the cover, which drops to 2.75 MPa after cover delamination (for the present example: μ_{fr} = 1, $f_{ct} = 0.33\sqrt{f_c'}$, N_b = 3). Due to the reversed cyclic nature of the displacement history, cover on the tension reinforcement is assumed to have delaminated or split if during the opposite direction of loading the compressive strain has attained the limit value of 0.003; this is used also in all other examples considered herein. The residual bond strength f_b^{res}

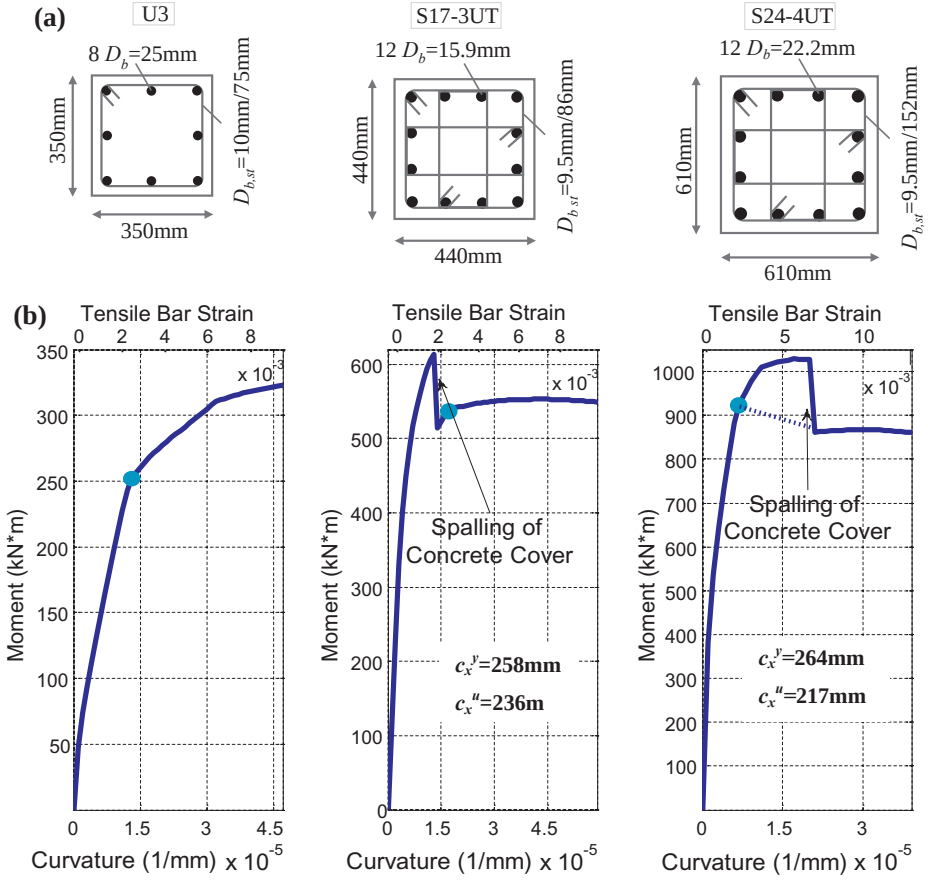

Fig. 6. For specimens U3, S17-3UT and S24-4UT (a) cross section details and (b) moment-curvature-tensile bar strain diagrams.

Table 1
Summary of the analyzed experiments (units: mm, MPa).

	Experimental details			Analysis		
Test ID	$\nu = N/(f_c' bd)$	Column geometry	Reinforcement	Anchorage	Shear span	Column deformation at ultimate
U3	0.16, $f_c' = 34.8$	Square section $h = 350$, $C_{cov} = 32.5$, $d = 305$, Sh. span $L_s = 1000$	Long: 8 evenly distributed bars, $D_b = 25$, $f_y = 430$, $E_{sh} = 5\%E_s$, Trans: 10@75, $f_{y,st} = 470$	$f_b^{max} = 1.25\sqrt{f_c'} = 7.40$, $s_1 = 0.2$, $L_b = 812$, $s_u^{anch}(x = 0) = 2.33$, $l_{r,u} = 313$	$f_b^{max} = 7.2$, $f_b^{res} = 1.44$, $s_1 = 0.2$, $\ell_{Do}^{max} = L_s + 12.5D_b = 1313$, $l_r = 319$, $\varepsilon_u = 0.0095$, $\phi_u = 4.7 \times 10^{-5}$, $c_x = 103$, $s_u^{span}(x = 0) = 2.36$	Total ℓ_{pl}: $\ell_{pl} = l_{r,u} + l_r = 632$ mm = 1.8 h, DR = 520 mm = 1.5 h, $\theta_u^{slip} = 0.018$, $\theta_u^f = \theta_y^f + \theta_{pl}^f = 0.015$, $\theta_u = 0.033 / \theta_u^{exp} = 0.035$
S17-3UT	0.5, $f_c' = 43.4$	Square section $h = 440$, $C_{cov} = 27$, $d = 405$, Shear span $L_s = 3049$	Long: 12 evenly distributed bars, $D_b = 15.9$, $f_y = 496$, $E_{sh} = 5\%E_s$, Trans: 9.5@86, $f_{y,st} = 496$	$f_b^{max} = 1.25\sqrt{f_c'} = 8.23$, $s_1 = 0.2$, $L_b = 890$, $s_u^{anch}(x = 0) = 1.50$, $l_{r,u} = 177$	$f_{b,wl/cov}^{max} = 11.49$ MPa, $f_{b,wo/cov}^{max} = 5.40$ MPa, $f_b^{res} = 20\%$ $f_b^{max} = 1.1$ MPa, $s_1 = 0.2$, $\ell_{Do}^{max} = L_s + 12.5D_b = 3248$, $l_r = 271$, $\varepsilon_u = 0.01$, $\phi_u = 5.9 \times 10^{-5}$, $c_x = 236$, $s_u^{span}(x = 0) = 2.30$	Total ℓ_{pl}: $\ell_{pl} = l_{r,u} + l_r = 448$ mm = h, DR = 450 mm = h, $\theta_u^{slip} = 0.012$, $\theta_u^f = 0.029$, $\theta_u = 0.041 / \theta_u^{exp} = 0.032$
S24-4UT	0.2, $f_c' = 36.5$	Square section $h = 610$, $C_{cov} = 49$, $d = 550$, Shear span $L_s = 3049$	Long: 12 evenly distributed bars, $D_b = 22.2$, $f_y = 400$, $E_{sh} = 1\%E_s$, Trans: 9.5@ 152, $f_{y,st} = 455$	$f_b^{max} = 1.25\sqrt{f_c'} = 7.55$, $s_1 = 0.2$, $L_b = 890$, $s_u^{anch}(x = 0) = 0.98$, $l_{r,u} = 80$	$f_{b,wl/cov}^{max} = 8.85$ MPa, $f_{b,wo/cov}^{max} = 2.0$ MPa, $f_b^{res} = 20\%$ $f_b^{max} = 0.4$ MPa, $s_1 = 0.2$, $\ell_{Do}^{max} = L_s + 12.5D_b = 3327$, $l_r = 301$, $\varepsilon_u = 0.013$, $\phi_u = 3.9 \times 10^{-5}$, $c_x = 217$, $s_u^{span}(x = 0) = 3.52$	Total ℓ_{pl}: $\ell_{pl} = l_{r,u} + l_r = 380$ mm = 0.6 h, DR = 350 mm = 0.57 h, $\theta_u^{slip} = 0.01$, $\theta_u^f = 0.017$, $\theta_u = 0.027/\theta_u^{exp} = 0.033$

Note: Test U3 by Saatcioglu and Ozcebe [29] and tests S17-3UT, S24-4UT by Bae and Bayrak [30]; DR = Damaged Region.

is defined as 20% of the maximum bond strength and parameter $s_1 = 0.2$ mm; s_2 mainly depends on the anchorage length which is equal to the shear span if the latter is transmitted to total disturbed region. For the present problem, s_2 is found equal to 0.5 mm at the ultimate state of reinforcement (see later in Fig. 8b).

After evaluation of the process of crack formation according with the proposed algorithm, the resulting distribution of strains is illustrated in Fig. 7. Note that stabilization of cracking occurred before yielding of the tensile bars (just after formation of the 4th crack). Ultimate strain corresponded to a disturbed region extending over the entire length of the column shear span including an equivalent additional length equal to $12.5D_b$ (313 mm) – thus $\ell_{Do}^{max} = L_s + 12.5D_b$ – in order to account for the end detail of reinforcement at the tip of the column being welded on a steel plate (this additional length is the anchorage length equivalent of a T-headed anchorage according to [28] – here this is a conservative estimate).

From Fig. 7 it is seen that the yield penetration length over the shear span at the last step of the calculation was 319 mm (0.91 h or $0.32L_s$) whereas the corresponding pullout slip was $s_u^{span}(x = 0) = 2.36$ mm (Fig. 8b). When including the yield penetration in the footing as is intended in the formal definition of ℓ_{pl} (Eq. (2b)) - the total plastic hinge length is 632 mm. (Note that the yield penetration length inside the footing is 313 mm or $0.029D_b f_y$ and the corresponding slip is $s_u^{anch}(x = 0) = 2.33$ mm, Fig. 8b.) Fig. 8a compares this value (i.e. 632 mm) with the empirical estimates of Eqs. (3a), (3b); the easy estimate of $0.5d$ is also noted. Also included is the result of the classical definition of plastic hinge length $(1 - M_y/M_u)L_s$. For comparison it is noted (red dashed line in Fig. 8a) that cover delamination was extended over 520 mm measured from the face of the support, according with the experimental report of specimen U3 [29]. Fig. 8b presents the slip distribution lengthwise the bar reinforcement, from where values at critical section are used next for the calculation of drift components.

The rotation components θ^{slip} and θ^f occurring at the critical section of the specimen at yielding and in the ultimate limit state are estimated according with Eqs. (1) and (2) by also adding the contribution from the anchorage [19]; here the theoretical ultimate point corresponds to the attainment of the maximum supportable disturbed length, $\ell_{Do}^{max} = L_s + 12.5D_b = 1313$ mm as described in the preceding. Thus, Eq. (1) is modified as follows:

$$\theta_y^{slip} = \underbrace{\frac{s_y^{span}}{d-0.4c_x}|_{x=0}}_{\text{shear span}} + \underbrace{\frac{s_y^{anch}}{d-0.4c_x}|_{x=0}}_{\text{anchorage}};\ \theta_u^{slip} = \underbrace{\frac{s_u^{span}}{d-0.4c_x}|_{x=0}}_{\text{shear span}} + \underbrace{\frac{s_u^{anch}}{d-0.4c_x}|_{x=0}}_{\text{anchorage}} \tag{20}$$

The values $s_y(x = 0)$ and $s_u(x = 0)$ are the contributions to slip at the base of the column resulting from pullout from the anchorage as well as from the shear span. For the analytical estimations of specimen U3, the compression zone depth was (Fig. 6b, $\varepsilon_u = 0.0095$ and $\phi_u = 4.7 \times 10^{-5}$ mm^{-1}) $c_x = 103$ mm (i.e., $d - 0.4c_x = 305–41 = 264$ mm) and from Eq. (20) the drift capacity owing to pullout slip was estimated as: $\theta_u^{slip} = 2.36/264 + 2.33/264 = 0.018$ rad. Using $\ell_r = 319$ mm, the ultimate rotation of the column due to flexure was: $\theta_u^f = \theta_y^f + \theta_{pl}^f$ where $\theta_y^f = \phi_y L_s/3$ (see also Eq. (2b)): $\theta_u^f = 1/3 \cdot 0.000013 \cdot 1000 + (0.000047 - 0.000013) \cdot 319 = 0.015$ rad. Term θ_u^{slip} accounts for 55% of the total rotation capacity of the RC column ($\theta_u = \theta_u^{slip} + \theta_u^f = 0.018 + 0.015 = 0.033$ rad). The experimental reported tip displacement at maximum moment (268 kN m) was 35 mm corresponding to a rotation of 0.035 rad.

4.1.2. Column S17-3UT [30]

The geometry of the column is summarized in Table 1 and depicted in Fig. 6a. The main bars were welded on a steel plate for the application of the load at the tip of the column. This was taken into account in the analysis by including a length of $12.5D_b$ (= 199 mm) as effective extension of the available development length in the shear span. Fig. 6b depicts the results of the moment – curvature - strain analysis. It is

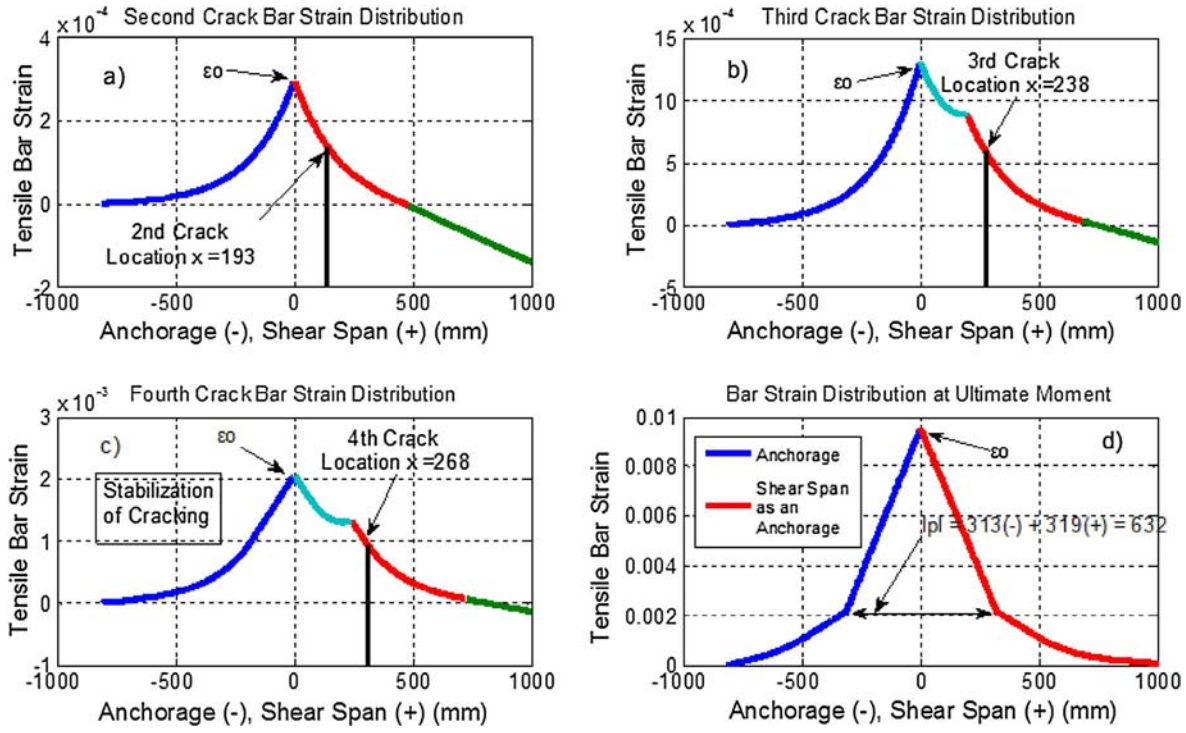

Fig. 7. For column U3 (a), (b), (c) tensile bar strain distributions along the anchorage (blue curves) and the shear span (cyan-red-green curves). Location of estimated successive cracks is indicated until crack stabilization. (d) Strain state of reinforcement at ultimate, where ℓ_{pl} is calculated. (For interpretation of the references to colour in this figure legend, the reader is referred to the web version of this article.)

evident that cover spalling occurs relatively early at a stage corresponding to bar yielding. For the shear span the maximum and the post-cover delamination values for bond strength were estimated from Eq. (19) as $f_{b,w/cov}^{\max} = 11.49$ MPa and $f_{b,wo/cov}^{\max} = 5.40$ MPa (indices *w/cov* and *wo/cov* correspond to the inclusion or not of the cover contribution). The process of detecting the crack formation and the corresponding strain distribution for the column are presented in Fig. 9. Stabilization of cracking occurred before yielding of the tensile bars. Moreover, after spalling of concrete cover, the contribution of the latter to bond strength was neglected (thus $f_b^{max} = f_{b,wo/cov}^{\max} = 5.40$ MPa).

As is evident from Fig. 9d the maximum sustained yield penetration length based on the proposed procedure is 271 mm (0.66 h or 0.09L_s) in the shear span and inside the footing it is 177 mm (or 0.022$D_b f_y$). Reported damage extended over a distance of 450 mm from the base of the column (see experimental reference, red dashed line in Fig. 8a). Fig. 8a presents the correlation of the analytical estimation with the empirical results and Fig. 8b the analytically estimated slip distribution lengthwise along the bar reinforcement at ultimate strain.

The rotation of the column at ultimate moment due to slippage θ_u^{slip} (Eq. (20)) is $\theta_u^{slip} = 2.30/311 + 1.5/311 = 0.012$ rad whereas the ultimate rotation of the column due to flexure (using $\ell_r = 271$ mm) is: $\theta_u^{flex} = 1/3 \cdot 0.000017 \cdot 3049 + (0.000059 - 0.000017) \cdot 271 = 0.029$ rad. Thus the total drift is estimated as 0.041 rad. The experimental curvature corresponding to 20% drop in lateral load capacity (this point was defined on the lateral load lateral displacement envelope after correction for the P-Δ effects), was 7×10^{-5} mm^{-1} (at the 6th level of cycling) and the associated drift was 0.032 rad.

4.1.3. Column S24-4UT [30]

Table 1 and Fig. 6a depict the geometric characteristics of the column specimen. As in the previous example, the effective development length of the longitudinal bars in the shear span was extended by 12.5D_b (= 278 mm) to account for welding of main reinforcement on a steel plate attached to the point load setup. Fig. 6b plots the calculated moment – curvature - strain diagram, indicating also the onset of cover delamination (beyond that point bond strength is reduced due to elimination of the cover contribution in Eq. (19)). For the shear span f_b^{max} was $f_{b,w/cov}^{\max} = 8.85$ MPa and $f_{b,wo/cov}^{\max} = 2.0$ MPa (with and without the cover contribution). The process of crack formation and the resulting bar strain distributions as calculated using the proposed algorithm are shown in Fig. 10.

From Fig. 10 it is shown that yield penetration length at maximum strain value $\varepsilon_u = 0.013$ is $l_r = 301$ mm (= 0.5 h or 0.1L_s) in the shear span. Adding the length of yield penetration in the footing (i.e. 80 mm or 0.01$D_b f_y$) the plastic hinge length is estimated at 380 mm. Fig. 8a presents the correlation of the analytical estimation with the empirical results and the reported damage into the shear span, extending up to a distance of 350 mm. Fig. 8b shows the estimated slip distribution lengthwise the bar reinforcement at ultimate strain.

Column rotation capacity at the ultimate moment was estimated as follows: from slip, $\theta_u^{slip} = 3.52/463 + 0.98/463 = 0.01$ rad and due to flexure $\theta_u^{flex} = 1/3 \cdot 0.000007 \cdot 3049 + (0.000039 - 0.000007) \cdot 301 = 0.017$ rad (in total 0.027 rad). The experimental reported drift ratio at to 20% net loss of lateral load strength was 0.033 rad (after correction of the result for the P-Δ effect); therefore the experimental total rotation of 0.033 rad was approximated adequately by the estimated analytical value of 0.027.

5. Parametric investigation

The parametric sensitivity of the proposed solution for the plastic hinge length is investigated in this section considering as a point of reference specimen U3 examined in the preceding section. Parameters considered, reference values, and ranges of parameters thereof are listed in Table 2; in each case one parameter is varied at a time keeping the reference values for all other variables (so the possible interaction effects between variables have not been considered in conducting the sensitivity analysis). Consistent with the original definition of the plastic hinge length (Eq. (2b)) the strain hardening ratio of the reinforcement E_{sh} effectively increases the plastic hinge length (Table 2).

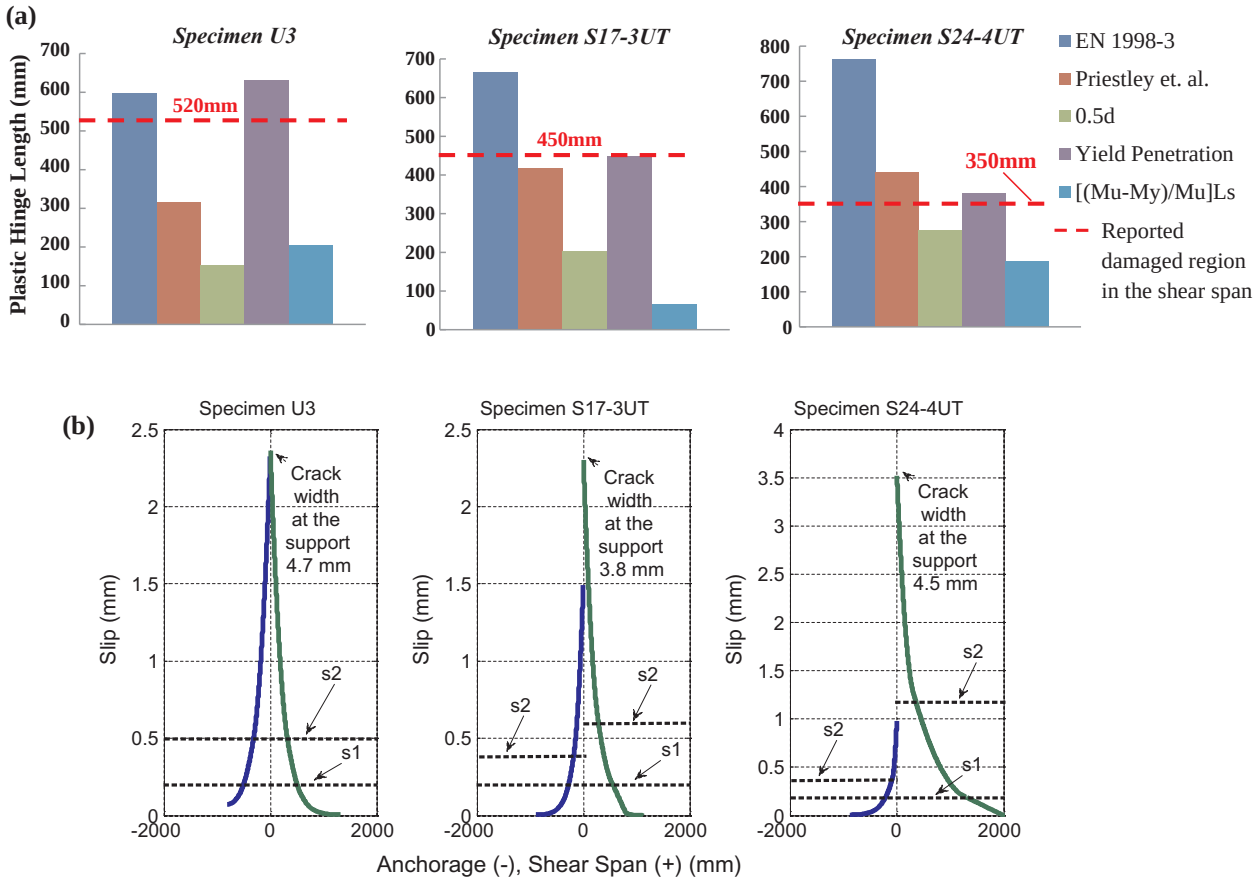

Fig. 8. For specimens U3, S17-3UT and S24-4UT (a) analytical calculation of the plastic hinge length ℓ_{pl} (purple bar) and its correlation with the design equations and (b) slip distributions along the bar length at ultimate strain (where ℓ_{pl} is calculated). (For interpretation of the references to colour in this figure legend, the reader is referred to the web version of this article.)

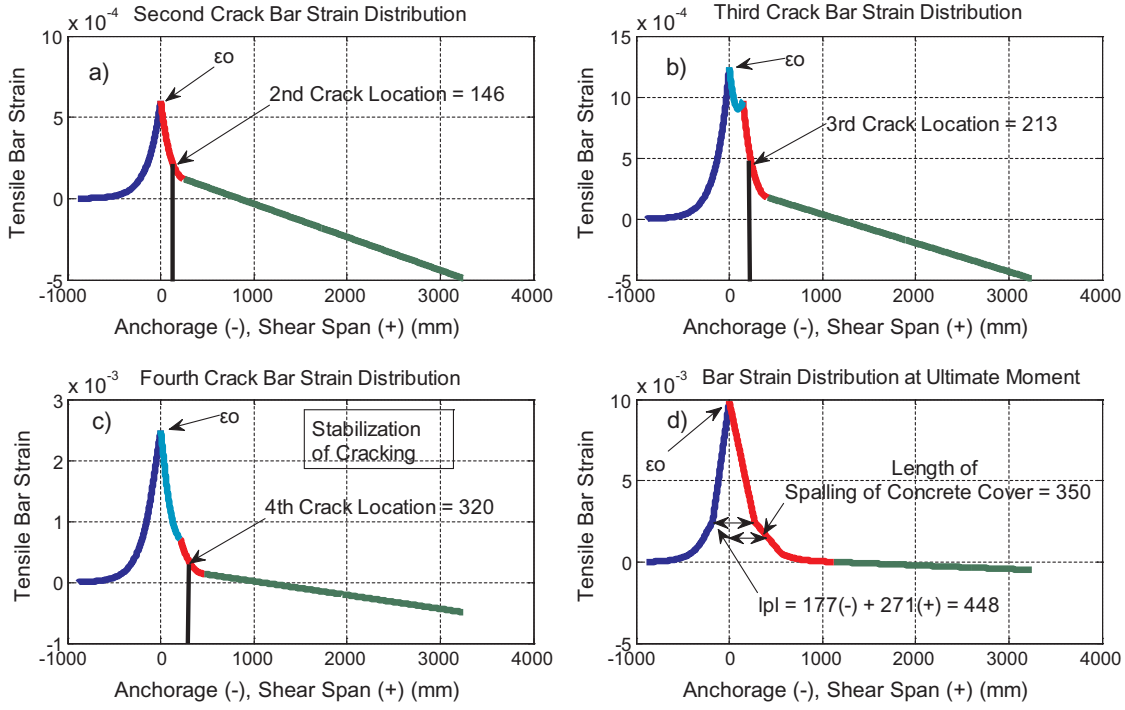

Fig. 9. For column S17-3UT (a), (b), (c) tensile bar strain distributions along the anchorage (blue) and shear span (cyan-red-green curves). Location of estimated successive cracks is indicated until crack stabilization. (d) Strain state of reinforcement at ultimate, where ℓ_{pl} is calculated. (For interpretation of the references to colour in this figure legend, the reader is referred to the web version of this article.)

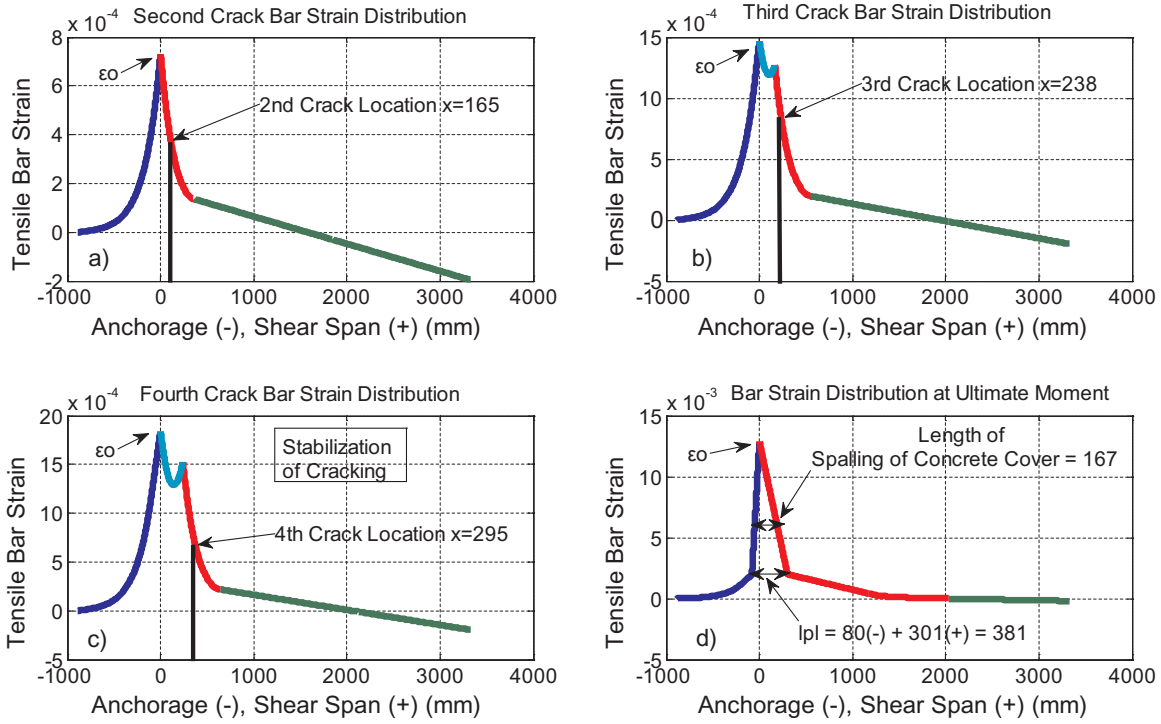

Fig. 10. For column S24-4UT (a), (b), (c) tensile bar strain distributions in the anchorage (blue) and the shear span (cyan-red-green curves). Location of estimated successive cracks is indicated until crack stabilization. (d) Strain state of reinforcement at ultimate, where ℓ_{pl} is calculated. (For interpretation of the references to colour in this figure legend, the reader is referred to the web version of this article.)

Similarly, a reduction of the residual bond strength f_b^{res} leads to further increase of the plastic hinge length (Table 2). It should be noted that the yield penetration length in the anchorage is included in the plastic hinge length.

The location of the cracks is affected by variable ω that defines the elastic bond according to Eq. (8). Decreasing the slip limit s_1 and increasing the value of average bond strength f_b^{max} both led to consolidation of the cracks closer to the critical section at the base of the column (before stabilization of cracking). In all analytical cases presented in Table 2 the first crack appears always at the base of the column ($x_{cr,1} = 0$), whereas in some of the experiments severe cracking occurred about 50 mm above the footing owing to the restraint provided by the footing, particularly when the drift history was applied by means of rotating that block while keeping the tip of the cantilever specimen stationary (e.g. [30]).

In the previous section three specimens with different aspect ratios (L_s/d) and axial load ratios [$\nu = N/(f_c bd)$] have been considered. The corresponding values for (L_s/d, ν) were, (3, 0.16), (7, 0.5), and (5, 0.2) respectively. Based on [30] the two parameters have a simultaneous effect on the extent of ℓ_{pl}, and a degree of interaction (i.e., the effect of L_s/d is pronounced only in the presence of high axial load ratio) (Tables 2, 3). To illustrate the sensitivity of the proposed approach in reproducing the experimental trend, a second reference point is introduced in the parametric study, namely the case of specimen U3 but with an axial load ratio of $\nu = 0.5$ (Table 3).

The mechanism by which the axial load ratio affects the damaged region is by accelerating and spreading delamination of the cover in the compression zone of the laterally swaying column. This was already evident in the M-ϕ-ε relationships of Fig. 6. Due to displacement reversals in the applied load history, compression and tension zones are sequentially interchanged. Thus, when the region with delaminated cover is placed in tension the bond strength of tension reinforcement is reduced significantly (the first term in the right hand side of Eq. (19) is seriously compromised) with commensurate implications on f_b^{res} also. From Eq. (18) it is evident that a larger ℓ_{pl} is expected under these conditions. To study this parametric trend consider the cross section of Fig. 11a. Cover delamination is assumed to occur when the compressive strain at the level of compression reinforcement reaches the limit of 0.004 (term $\xi = c_x/d$ is the normalized compression zone and $\xi' = d_2/d$ defines the position of the compression reinforcement as per the extreme fiber). In this case, from cross section analysis, the strain of the tensile reinforcement ε_o is given by Eq. (21).

$$\varepsilon_o = 0.004 \cdot \frac{1-\xi}{\xi-\xi'} \tag{21}$$

For the needs of the parametric investigation the relationship between ν and ε_o is established using experimental evidence: the column test series conducted by Watson and Park [16] included specimens with various axial load ratios ranging from $\nu = 0.1$ to 0.6. Based on the reported test results, the relation between axial load ν and normalized

Table 2
Parametric Investigation – Properties similar to specimen U3 (units: mm, MPa).

Parameter	$\nu = N/(f_c' bd) = 0.15$	$\nu = N/(f_c' bd) = 0.3$	$\nu = N/(f_c' bd) = 0.5$
Plastic Hinge Length	1.8 h	1.3 h	0.9 h
Parameter	$f_b^{max} = 3$	$f_b^{max} = 5$	$f_b^{max} = 7$
Plastic Hinge Length	3.1 h	2.2 h	1.8 h
Parameter	$f_b^{res} = 1$	$f_b^{res} = 2$	$f_b^{res} = 3$
Plastic Hinge Length	2.2 h	1.6 h	1.3 h
Parameter	$E_{sh} = 1\%E_s$	$E_{sh} = 2.5\%E_s$	$E_{sh} = 5\%E_s$
Plastic Hinge Length	0.4 h	0.9 h	1.8 h
Parameter	$L_s = 2$ h	$L_s = 3$ h	$L_s = 4$ h
Plastic Hinge Length	1.8 h	1.8 h	1.8 h
Parameter		$D_b = 18$	
Plastic Hinge Length		1.4 h	

Table 3
Parametric Investigation – Axial load ratio equal to 0.5 (units: mm, MPa).

Ideal reference case	$\nu = N/(f_c' bd) = 0.5$; *all other characteristics are those of U3*		
Parameter	$f_b^{max} = 3$	$f_b^{max} = 5$	$f_b^{max} = 7$
Plastic Hinge Length	1.6 h	1.1 h	0.9 h
Parameter	$f_b^{res} = 1$	$f_b^{res} = 2$	$f_b^{res} = 3$
Plastic Hinge Length	1.1 h	0.8 h	0.7 h
Parameter	$E_{sh} = 1\%E_s$	$E_{sh} = 2.5\%E_s$	$E_{sh} = 5\%E_s$
Plastic Hinge Length	0.1 h	0.4 h	0.9 h
Parameter	$L_s = 2$ h	$L_s = 3$ h	$L_s = 4$ h
Plastic Hinge Length	0.9 h	0.9 h	0.9 h
Parameter	$D_b = 18$		
Plastic Hinge Length	0.7 h		

compression zone depth ξ is estimated as, $\xi = 0.25\nu + 0.07$ (Fig. 11b). Thus, given the applied axial load ν, the normalized compression zone depth ξ of the cross section is estimated; then, the corresponding strain in the tension reinforcement at the critical section, ε_o, is obtained from Eq. (21). This is substituted in Eq. (18) to define the yield penetration length into the shear span, using different intensities of average residual bond strength depending on the magnitude of axial load (lower residual bond strength for higher axial load to reflect the effect of delaminated cover over a broader region). This procedure is visualized in the combined diagram of Fig. 11c, where curves of ν - ε_o (grey curve) and l_r/d - ε_o (black lines, where the thicker the curve the higher the f_b^{res} is) are simultaneously plotted. Note that the horizontal grey dashed line drawn at the upper part of Fig. 11c defines the available column aspect ratio, L_s/d which serves as the ultimate limit for possible penetration. This diagram may be used to illustrate two aspects of the parametric sensitivity of the problem: a) the increase of axial load for example from 0.2 to 0.4 (following the red arrow) results in reduction of the strain capacity of the cross section (from 0.05 to 0.027) along with diminishing of the f_b^{res} (crossing from the thicker to the thinner curve, i.e. from 4 to near 1 MPa) as well as an increase of the extent of the plastic hinge length in the shear span (i.e. from 1.1 to 2.3d, where d is the effective depth of the cross section, see the red dashed horizontal lines). (b) the unified diagram ν - l_r/d - ε_o can be used in design: given the axial load and the aspect ratio of the member, the strain capacity of the cross section and the corresponding plastic hinge length are uniquely defined, leading to proper assessment of the members' available deformation capacity. The extent and intensity of damage may be effectively reduced through confinement as a higher value of the residual bond strength may be supported (see the black dashed paths in Fig. 11c).

6. Conclusions

Yield penetration occurs from the critical section towards both the shear span and the support of columns; physically it refers to the extent of the nonlinear region and determines the pullout slip measured at the

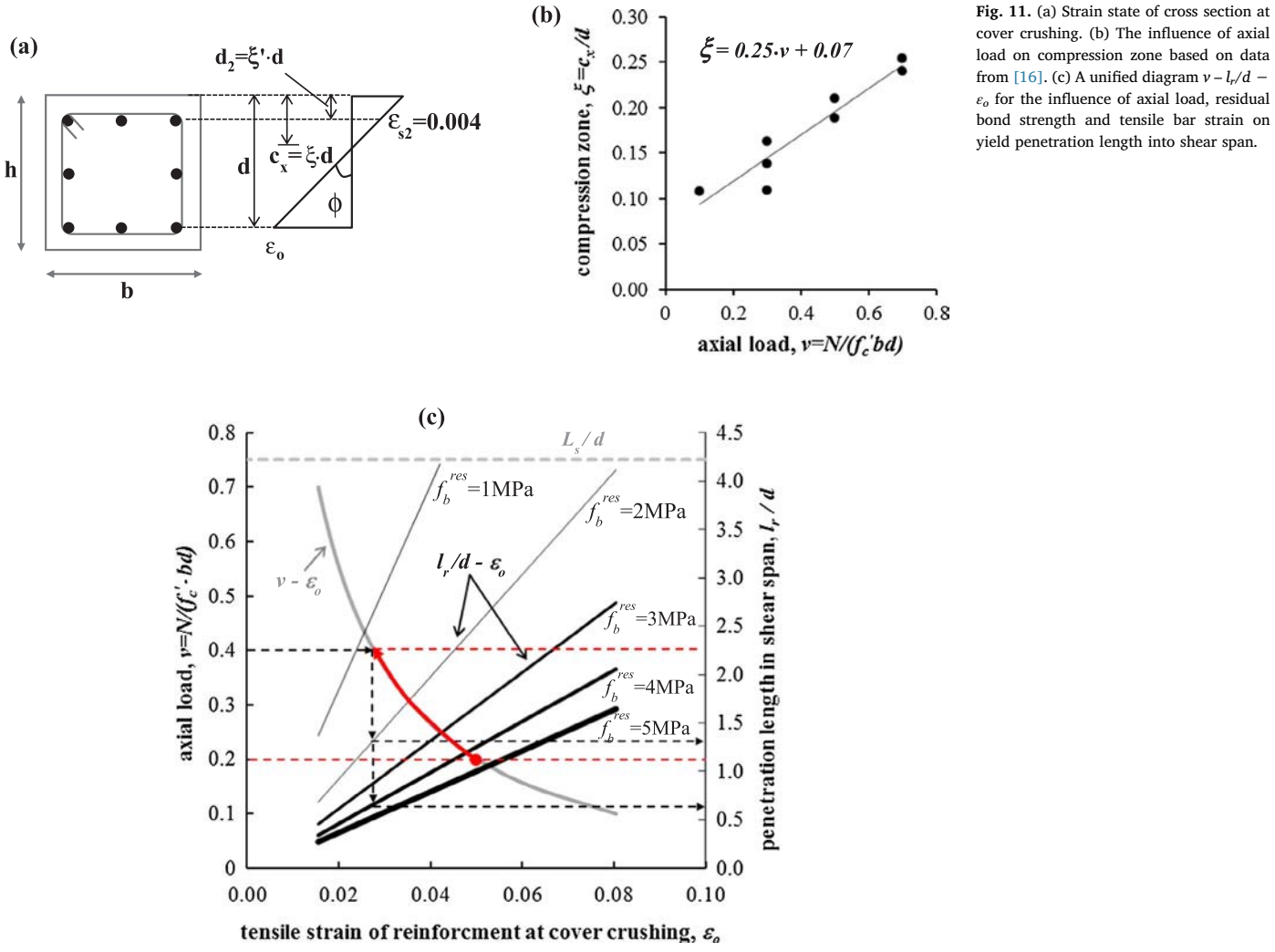

Fig. 11. (a) Strain state of cross section at cover crushing. (b) The influence of axial load on compression zone based on data from [16]. (c) A unified diagram $\nu - l_r/d - \varepsilon_o$ for the influence of axial load, residual bond strength and tensile bar strain on yield penetration length into shear span.

critical section. Contrary to the fixed design values adopted by codes of assessment, the yield penetration length is actually the only consistent definition of the notion of the plastic hinge length, whereas the latter determines the contribution of pullout rotation to column drift and column stiffness. In order to establish the plastic hinge length in a manner consistent to the above definition, this paper pursued the explicit solution of the field equations of bond over the shear span of a column. Through this approach, the bar strain distributions and the extent of yield penetration from the yielding cross section towards the shear span were resolved and calculated analytically. By obtaining this solution a consistent definition of plastic hinge length is established, by reference to the state of reinforcement strain (replacing the stress based definition used previously). The true parametric sensitivities of this design variable for practical use in seismic assessment of existing structures are illustrated. The numerical results show good agreement with the experimental evidence and are consistent with the experimental trends supported by test databases, confirming that the plastic hinge length is controlled by the residual bond that may be mobilized along the yielded reinforcement.

Acknowledgements

The first author would like to thank the Alexander S. Onassis Public Benefit Foundation whose financial support is greatly appreciated.

References

[1] Pantazopoulou SJ. Seismic Assessment and Retrofit of Reinforced Concrete Buildings. fib Bulletin No. 24 Chapter 4, Case Postale 88, CH-1015, Lausane, Switzerland; 2003.
[2] Inel M, Aschheim M, Pantazopoulou S. Deformation Indices for Concrete Columns: Predicted vs. Measured. 13thWorld Conf. on Earthquake Engineering, Vancouver, Canada, No. 2397. 2004.
[3] Pantazopoulou SJ, Syntzirma DV. Deformation Capacity of Lightly Reinforced Concrete Members – Comparative Evaluation. In Advances in Performance-Based Earthquake Engineering (ACES workshop), Springer Pubs., (Ed.: M.N.Fardis); 2010.
[4] ASCE/SEI 41. Seismic Rehabilitation of Existing Buildings. American Society of Civil Engineers, Reston, VA; 2007.
[5] EN 1998-3. Eurocode 8: Design of structures for earthquake resistance -Part 3: Assessment and retrofitting of buildings. European Committee for Standardization (CEN), Brussels; 2005.
[6] Panagiotakos TB, Fardis MN. Deformations of reinforced concrete members at yielding and ultimate. ACI Struct J 2001;98(2):135–48.
[7] Biskinis D, Fardis M. Models for FRP-wrapped rectangular RC Columns with Continuous or Lap-Spliced Bars Under Cyclic Lateral Loading. Eng Struct 2013;57:199–212. Elsevier.
[8] Whitney CS. Design of reinforced concrete members under flexure and combined flexure and direct compression. ACI J 1937;33:483–98.
[9] Moehle JP. Displacement-based design of rc structures subjected to earthquakes. Earthquake Spectra 1992;8(3):403–28.
[10] EN 1998-1. Eurocode 8: Design of structures for earthquake resistance – Part 1: General rules seismic actions and rules for buildings, European Committee for Standardization (CEN), Brussels; 2004.
[11] Priestley MJN, Park R. Strength and ductility of bridge substructures. RRU Bull. No. 71, Road Res. Unit, National Roads Board, Wellington, New Zealand; 1984.
[12] Priestley MJN, Park R. Strength and ductility of concrete bridge columns under seismic loading. ACI Struct J 1987;84(1):61–76.
[13] Priestley MJN, Seible F, Calvi M. Seismic Design and Retrofit of Bridges. N. York: J. Wiley & Sons Inc; 1996.
[14] Lehman DE, Lynn AC, Aschheim MA, Moehle JP. Evaluation methods for reinforced concrete columns and connections. 11th World Conference on Earthquake Engineering, Acapulco, Mexico, June 23–28, Paper No. 673; 1996.
[15] Bae S, Bayrak O. Plastic hinge length of reinforced concrete columns. ACI Struct J 2008;105(3):291–300.
[16] Watson S, Park R. Simulated seismic load tests on reinforced concrete columns. ASCE J Struct Eng 1994;120(6):1825–49. June.
[17] Syntzirma DV, Pantazopoulou SJ. Deformation capacity of r.c. members with brittle details under cyclic loads. ACI Special Publication 236, “Seismic Shear”, published by ACI-ASCE Committee 445, CD-ROM; 2007.
[18] Syntzirma DV, Pantazopoulou SJ, Aschheim M. Load history effects on deformation capacity of flexural members limited by bar buckling. ASCE J Struct Eng 2010;136(1):1–11.
[19] Tastani SP, Pantazopoulou SJ. Yield penetration in seismically loaded anchorages: effects on member deformation capacity. Techno Press Earthquake Struct 2013;5(5):527–52.
[20] Tastani SP, Pantazopoulou SJ. Reinforcement and concrete bond: State determination along the development length. ASCE J Struct Eng 2013;139(9):1567–81.
[21] Filippou F, Popov E, Bertero V. Modeling of R/C joints under cyclic excitations. ASCE J Struct Eng 1983;109(11):2666–84.
[22] Tassios TP, Yannopoulos PJ. Analytical studies on reinforced concrete members under cyclic loading based on bond-slip relationships. ACI Mater J 1981;78(3):206–16.
[23] Bonacci J, Marquez J. Tests of Yielding Anchorages under Monotonic Loadings. ASCE J Struct Eng 1994;120(3):987–97.
[24] Bigaj AJ. Structural Dependence of Rotation Capacity of Plastic Hinges in RC Beams and Slabs PhD Thesis Delft, the Netherlands: Faculty of Civil Engineering, Delft University of Technology; 1999.
[25] MacGregor J, Wight J. Reinforced concrete mechanics and design. New Jersey, USA: Pearson Education, Inc., Upper Saddle River; 2005. 0-13-142994-9.
[26] Martin-Pérez B, Pantazopoulou SJ. Effect of bond, aggregate interlock and dowel action on the shear strength degradation of reinforced concrete. Elsevier, Eng Struct 2001;23:214–27.
[27] EN 1992-1-1 (2004): Eurocode 2: Design of concrete structures – Part 1–1: General rules and rules for buildings, European Committee for Standardization (CEN), Brussels; 2004.
[28] Fib Model Code. Chapter 6: Interface Characteristics. Berlin, Germany: Ernst & Sohn Publications; 2010. p. 434.
[29] Saatcioglu M, Ozcebe G. Response of reinforced concrete columns to simulated seismic loading. ACI Struct J 1989;86(1):3–12.
[30] Bae S, Bayrak O. Seismic performance of full-scale reinforced concrete columns. ACI Struct J 2008;105(2):123–33.
[31] Scott BD, Park R, Priestley MJN. Stress-strain behavior of concrete confined by overlapping hoops at low and high strain rates. ACI J 1982;79:13–27.
[32] Hognestad E. A Study of Combined Bending and Axial Load in Reinforced Concrete Members. Bulletin No. 399, Engineering Experimental Station, University of Illinois; 1951.
[33] Tastani SP, Pantazopoulou SJ. Direct tension pullout bond test: experimental results. ASCE Struct Eng 2010;136(6):731–43.